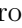











# Microwave surface resistance of Tl-1223 films in a dc magnetic field

Alessandro Magalotti , Student Member, IEEE, Andrea Alimenti , Member, IEEE, Emilio Bellingeri , Cristina Bernini , Sergio Calatroni , Member, IEEE, Alessandro Leveratto , Enrico Silva , Senior Member, IEEE, Kostiantyn Torokhtii , Member, IEEE, Ruggero Vaglio , Pablo Vidal García , Member, IEEE, Nicola Pompeo , Senior Member, IEEE,

**Abstract**—We present first preliminary surface impedance measurements on Tl-1223 films in dc magnetic fields, in view of potential applications for the next generation Future Circular Collider (FCC-hh) at CERN. The Tl-1223 samples were produced through laser ablation, with nominal thickness of 1  $\mu\text{m}$  and grown on a thick  $\text{LaAlO}_3$  substrate. The presence of Tl-1212 phase identified by XRD and BSE microscopy, could be avoided by changing the oxygen partial pressure during heat treatment. The high-frequency transport properties of the samples were characterized using microwave resonant devices, at fixed frequencies of 14.9 GHz, 24.2 GHz and 26.7 GHz, in the temperature range 40 K to 140 K. An external applied static magnetic field up to 12 T was applied. Samples from subsequent batches exhibited huge improvements in the microwave properties, confirming the progress in the deposition technique.

**Index Terms**—Cuprates, Laser ablation, Microscopy, Microwave devices, Surface impedance, Thick films, Superconducting materials growth

## I. Introduction

RECENTLY, the microwave electrical conductivity of high temperature superconductors (HTS) in the mixed state became of great interest. Indeed, there is a strong motivation at CERN to understand whether HTS can be used to replace copper as a coating of the beam screen for the operation of next-generation particle accelerators, such as the Future Circular Collider (FCC-hh) [1]. To mitigate the particles bunches instabilities and carry the beam-induced image currents (up to a few GHz), low surface resistance  $R_s$  is required for the beam screens. However, the need to operate in very

strong static magnetic fields up to 14 T and at cryogenic temperatures in the range 50 K to 70 K [2], [3], and the requirement of direct deposition of superconducting coatings onto the beam screen, put severe challenges in the identification of suitable materials. Interesting candidates are thallium-based cuprate superconductors, since they can reach extremely high critical temperatures ( $T_c$ ): in particular, Tl-1223 has a nominal  $T_c$  of 125 K [4], which would allow in principle operation at higher temperatures than, *e.g.*, YBCO. Moreover, thallium cuprates could also be electrochemically deposited [5], allowing the deposition process to be rapidly scaled up to an industrial level, as it will be necessary to cover a circumference length of about 90 km of beam screen.

In this work, we report the progress made in the deposition of Tl-1223 films and we discuss and compare the microwave properties of two Tl-1223 samples coming from different batches, after optimization of the deposition conditions. A huge progress is evident among the different batches. By optimizing the deposition process it was possible to avoid the presence of different phases, and only the Tl-1223 phase is present in the latest sample. This progress was accompanied by substantial improvements in the microwave performances, leading to a reduction of the surface resistance  $R_s$  by a factor  $\sim 10$  and a much stronger resilience in a magnetic field.

## II. Samples realization

### A. Film deposition and growth

$\text{Tl}_{0.7}\text{Pb}_{0.2}\text{Bi}_{0.2}\text{Sr}_{1.6}\text{Ba}_{0.4}\text{Ca}_{1.9}\text{Cu}_3\text{O}_{9+x}$  (Tl-1223) films, whose stoichiometry has been optimized to increase the irreversibility field  $H_{irr}$  [5], [6], were grown with a Solid-Phase Epitaxy Process. Single-crystal  $\text{LaAlO}_3$  (001) substrates ( $10 \times 10 \times 0.5 \text{ mm}^3$ ) were used. This substrate material was selected due to its proven compatibility with Tl-based cuprates [7], [8] and its suitability for microwave measurements, as its dielectric permittivity remains nearly constant over a wide temperature range. Precursor films were deposited on the substrates from an homemade target prepared as described in [6] using a pulsed laser deposition (PLD) system equipped with a Nd:YAG laser ( $\lambda = 1064 \text{ nm}$ ) operating at an energy density of approximately  $2 \text{ J} \cdot \text{cm}^{-2}$ . The laser repetition rate was maintained at 5 Hz, and the target-to-substrate distance was fixed at 3 cm. The deposition was performed in an oxygen-rich atmosphere to promote partial oxidation of the precursor materials, with a pure oxygen partial pressure ranging

Received 13 October 2025; revised 12 January 2026; accepted 2 February 2026. Date of publication 9 February 2026; date of current version 13 February 2026. This work was supported in part by the FCC collaboration under MoU Addendum under Grant FCC-GOV-CC-0218 and Grant KE5084/ATS, and in part by CERN Funding Addendum under Grant FCC-GOV-CC-0217 and Grant KE5072/TE through the FCC study. (Corresponding author: Alessandro Magalotti.)

Alessandro Magalotti, Andrea Alimenti, Enrico Silva, Kostiantyn Torokhtii, Pablo Vidal García, and Nicola Pompeo are with the Department of Industrial, Electronic and Mechanical Engineering, Roma Tre University, 00154 Rome, Italy (e-mail: alessandro.magalotti@uniroma3.it; nicola.pompeo@uniroma3.it).

Emilio Bellingeri, Cristina Bernini, and Alessandro Leveratto are with the SPIN-CNR, 16152 Genova, Italy.

Sergio Calatroni is with the CERN, 1211 Geneva, Switzerland.

Ruggero Vaglio is with the SPIN-CNR, 16152 Genova, Italy, and also with the Department of Physics, University of Naples Federico II, 80138 Naples, Italy.

Color versions of one or more figures in this article are available at <https://doi.org/10.1109/TASC.2026.3662298>.

Digital Object Identifier 10.1109/TASC.2026.3662298

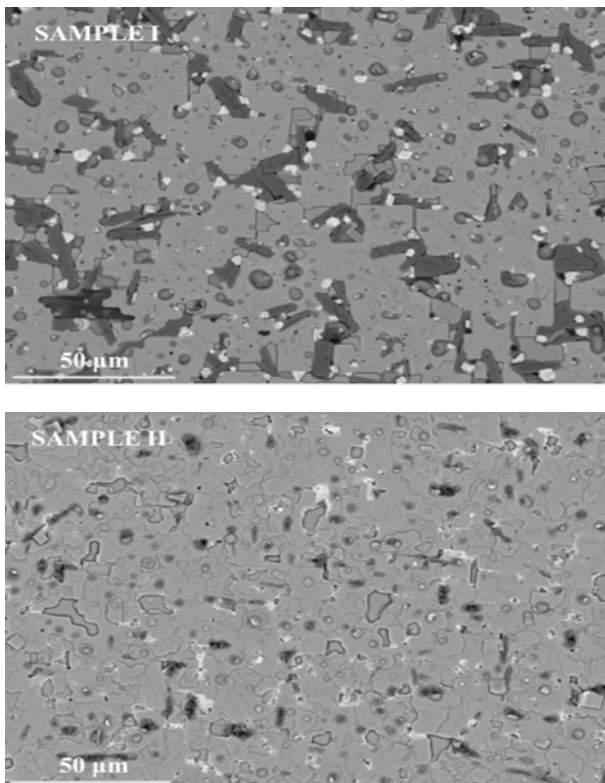


Fig. 1. BSE images of Tl-1223 films grown on  $\text{LaAlO}_3$  (001). The top panel (Sample I) shows uniform surface coverage by Tl-1223 grains (light gray) together with dark-gray and white secondary crystals attributed to complex oxide formation. The bottom panel (Sample II) also exhibits good surface coverage, with a noticeably reduced presence of secondary oxides.

from 10.7 Pa to 146.7 Pa in an ultra-high-vacuum (UHV) base pressure of  $1.3 \times 10^{-6}$  Pa. The resulting film thickness for all samples was set to 1  $\mu\text{m}$ . After deposition, the samples were subjected to a high-temperature reaction in a high-pressure furnace. The reaction was carried out at 950  $^\circ\text{C}$  for 3 h under a static total pressure of  $5 \times 10^6$  Pa of pure Ar, with a partial pressure of  $25 \times 10^3$  Pa to  $50 \times 10^3$  Pa of  $\text{O}_2$ . This high-pressure environment was designed to stabilize the thallium phase and promote epitaxial film growth. Two sample series were prepared, each differing slightly in oxygen partial pressure during the reaction step. Sample I and Sample II were processed under  $40 \times 10^3$  Pa and  $25 \times 10^3$  Pa of  $\text{O}_2$ , respectively, resulting in differences in film quality. As reported in [6], the stability range for obtaining a pure Tl-1223 phase is extremely narrow, and small deviations can lead to the formation of competing Tl-1212 or mixed phases.

### B. Structural, morphological and DC transport characterization

A comparative analysis of Sample I and Sample II was performed. Figure 1 presents the Back-Scattered Electron (BSE) micrographs of the two films. A slight reduction in oxygen partial pressure during processing led to decreased formation of secondary oxide phases that tend to segregate between Tl-1223 grains. Based on Scanning

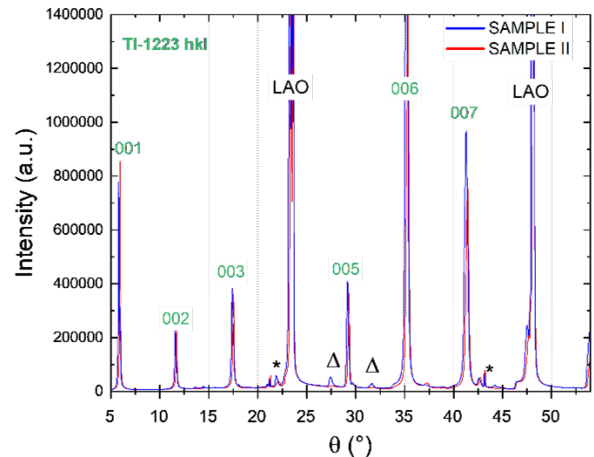


Fig. 2. X-ray diffraction patterns of Tl-1223 films on  $\text{LaAlO}_3$  (001). The 001 peaks confirm strong c-axis orientation of the Tl-1223 phase. Secondary oxides are marked with stars  $*$ , while the Tl-1212 phase, more pronounced in Sample I, is indicated by  $\Delta$  (102 and 103 reflections).

Electron Microscopy (SEM) and Energy Dispersive X-ray analysis (not shown here), two main secondary complex oxides were identified:  $\text{SrCaCu}_3\text{O}_5$  and a copper-free phase rich in barium and bismuth, attributed to  $\text{SrCaBi}_2\text{Ba}_3\text{O}_x$ . These phases are clearly visible in Figure 1, where BSE images show dark-gray and white crystals, respectively. Indeed, in Sample II the oxide phase is significantly reduced and localized mainly at the film surface. These observations indicate that a lower oxygen partial pressure during heat treatment limits oxygen incorporation, leading to smaller grain size and fewer surface oxides. X-ray diffraction (XRD) analysis (Figure 2) confirms the growth of Tl-1223 with a strong 001 c-axis texture and the presence of secondary oxides (marked with stars). While the differences between Sample I and Sample II are less pronounced than in the SEM images, XRD reveals a slightly higher fraction of Tl-1212 in Sample I. This phase, which lacks c-axis orientation, is indicated by the 102 and 103 peaks ( $\Delta$ ). The combined SEM and XRD analyses provide complementary insights into the microstructure and phase purity of the film. DC transport measurements of resistance as a function of temperature show that both samples exhibit similar behavior, with a relatively sharp superconducting transition around 116 K (Figure 3). Despite the presence of a minor Tl-1212 phase, the observed transition is primarily attributed to the majority Tl-1223 phase, which is well connected throughout the film.

### III. Microwave measurements: methods

We measure and compare the microwave surface resistance of the two Tl-based samples with different growth processes discussed above, with the clarification that Sample II has been actually replaced by a twin.

The surface resistance is the real part of the complex surface impedance  $Z_s = R_s + iX_s$  [9], which represents the measurable response function of a material to an

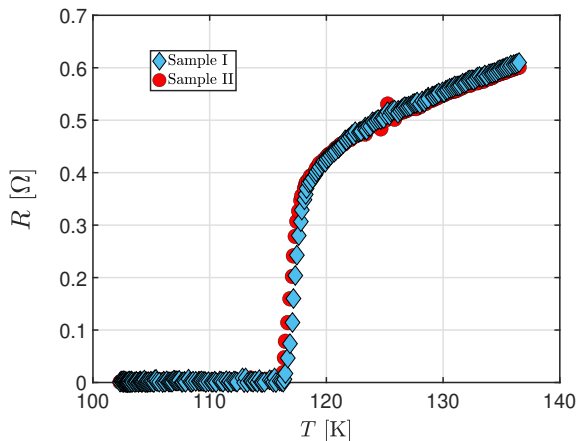


Fig. 3. Resistance vs temperature for Tl-1223 films on LaAlO<sub>3</sub> (001). Both samples show sharp superconducting transitions at  $\sim 116$  K, due to the Tl-1223 phase.

electromagnetic field. The surface impedance is affected by the geometry of the material: when the penetration depth of the conducting/superconducting material, grown on a highly resistive material, exceeds the thickness of the superconducting coating,  $Z_s$  is directly expressed as  $Z_s = \rho/t$ , where  $\rho$  is the material complex resistivity and  $t$  its thickness [10]. By contrast, when the thickness of the conducting or superconducting coating exceeds the penetration depth, one has (in the local limit)  $Z_s = \sqrt{2\pi f \mu_0 \rho}$ , where  $f$  is the frequency and  $\mu_0$  is the magnetic permeability of vacuum. In our Tl-1223 thick films, in the normal state the electromagnetic penetration length (skin depth)  $\delta = (2\rho_n/2\pi f \mu_0)^{-1/2}$  is larger than  $t$ , so that  $R_{s,n} = \rho_n/t$ . By contrast, in the superconducting state the London penetration depth cannot be assumed larger than  $t$ . Moreover, in the mixed state the e.m. penetration depth is a complex function of temperature and magnetic field [11], [12] and thus  $R_s$  cannot be expressed by a simple function of  $\rho$ . In the following we will present raw data for  $R_s$ , recalling that only above  $T_c$  they are directly related to  $\rho_n$ .

The measuring technique, already extensively discussed in previous works [13], [14], involves a pillbox-like dielectric loaded resonator. A dielectric puck is hosted by a copper cavity, and the Tl-1223 film replaces part of one of the flat walls. Depending on the combination of the dielectric crystal and resonator materials and dimensions selected, quasi-transverse electric modes (TE) were excited at different frequencies. Typical values are: cavity radius = 12 mm; crystal material = Al<sub>2</sub>O<sub>3</sub>; crystal radius = 4 mm. Sample I was measured at 26.7 GHz (TE<sub>021</sub> mode) in a low-field (1.2 T) cryostat, while the improved Sample II was measured in a high-field cryostat with a resonator operating on TE<sub>011</sub> and TE<sub>021</sub> modes, at the frequencies of 14.9 GHz and 24.2 GHz, respectively. The temperature was swept from 40 K up to 140 K and the magnetic field up to  $\mu_0 H = 1.2$  T or 12 T. The microwave measurements

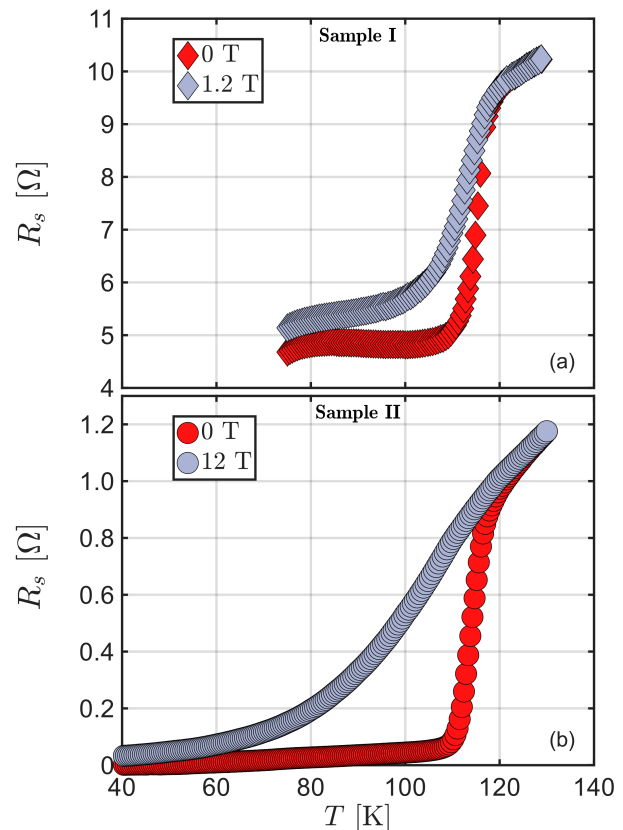


Fig. 4. Temperature dependence of  $R_s$ , with and without a magnetic field. (a) Sample I,  $f = 26.7$  GHz,  $\mu_0 H = 0$  T and 1.2 T. (b) Sample II,  $f = 14.9$  GHz,  $\mu_0 H = 0$  T and 12 T. Note in Sample I the large residual resistance, the large absolute value of  $R_s$  and the strong effect of a moderate magnetic field, and in Sample II the absence of all those effects, with particular attention to the strong magnetic resilience.

were performed with a ZVA 40 Rhode & Schwarz vector network analyzer, connected to the resonator via cryogenic and non-magnetic coaxial cables. Quality factor  $Q$  of the resonator was collected as a function of  $T$  and of the applied magnetic field  $H$ . Temperature- and field-induced changes of the quality factor reflected changes in the surface resistance of the sample. A calibration of the bare cavity was used to extract the absolute surface resistance. Since the resonator is made of copper, absolute  $R_s$  are affected by a large (systematic) uncertainty of several m $\Omega$ . Such effect is of no particular relevance in the present case where the application of a magnetic field determines large dissipation (differently from high-resolution  $R_s$  measurements in superconductors for accelerating cavities). A comprehensive description of the measuring chain can be found in [13], where it is shown how to extract the superconductor  $Z_s$  from the resonator microwave characterization.

#### IV. Results

The temperature dependence of  $R_s$  in nominally zero field and with the application of a magnetic field perpendicular to the sample surface are reported in Figure 4. We first comment on the measurements in zero dc field. As it

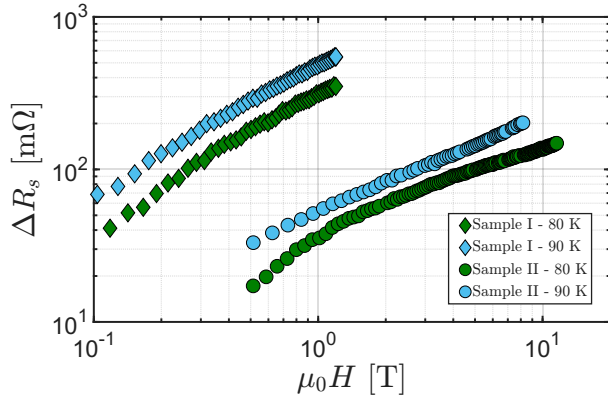


Fig. 5. Field-induced change  $\Delta R_s$  at fixed temperatures of 80 K and 90 K measured at  $f = 26.7$  GHz and 24.2 GHz for Sample I and II, respectively.

can be seen, large discrepancies emerge both in the normal and in the superconducting state among the two samples. Although both samples exhibit a high critical temperature  $T_c \approx 118$  K, corresponding to the Tl-1223 superconducting phase, Sample I (red diamonds in Figure 4a) shows clear traces of a second phase with  $T_{c,2nd} \approx 80$  K, corresponding to the undesired Tl-1212 phase, in agreement with XRD and BSE measurements in Section II. Moreover, Sample I has an anomalously large normal state  $R_{s,n} \approx 10 \Omega$ . Using the thin film approximation, with nominal thickness  $t = 1 \mu\text{m}$  one would get a normal state resistivity (see Section III)  $\rho_n = R_s t \approx 1 \text{ m}\Omega \text{ cm}$ , a rather large value among the literature data [15]–[17]. Moreover, a very large residual surface resistance of  $\sim 5 \Omega$  appears at 78 K. The results on Sample I point then to a rather inhomogeneous sample. We remind that the microwave surface resistance is a volume probe in thin films. The emerging framework is then of a sample where the Tl-1223 phase is present in a sufficient part of the volume to give a well-detectable microwave transition, it is well connected so that a sharp dc resistive transition could be measured, but it is accompanied by large portions of other phases and possibly large defects originating from the unmatched lattice mixture of Tl phases, that give the large residual  $R_s$ . By contrast, Sample II (red circles in Figure 4b) is exempt from all these issues. The normal state resistivity is estimated as  $\rho_n = R_s t \approx 100 \mu\Omega \text{ cm}$ , a typical value for cuprates although on the lower edge of the reported values for Tl-1223 [15]–[17]. No particular residual  $R_s$  is detected, and no clear signatures of second superconducting phases exist.

We now comment on the response to a dc magnetic field. As is apparent from Figure 4, the application of a dc magnetic field has a very different effect on Sample I and Sample II. In Sample I a moderate field  $\mu_0 H = 1.2$  T produces a quite significant widening of the superconducting transition (gray diamonds in Figure 4a), while in Sample II a very strong magnetic field of  $\mu_0 H = 12$  T determines a widening of the transition (gray circles in Figure 4b) that is not much larger than that produced by a small field

in Sample I. Sample II appears then much more resilient with respect to the application of a dc magnetic field, a feature beneficial for the envisioned application for the FCC beam screen.

To better appreciate the field dependence of  $R_s$  in Tl-1223 samples, we report in Figure 5 the field dependence of the field-induced change in the surface resistance,  $\Delta R_s = R_s(H) - R_s(0)$ , collected at 80 K and 90 K in both samples. We observe the same  $R_s$  reduction factor  $\sim 10$  at both temperatures at 1 T. Here the data are measured at frequencies close enough so to avoid frequency-induced effects. In addition to the smaller absolute values of  $R_s$  in Sample II, even at larger fields, we observe also a weaker field dependence (note the log scale). This is a further indication that the improvement of the sample crystalline quality led to a significantly stronger resilience with respect to the application of a magnetic field.

## V. Comparison with Copper

The possible choice of Tl-1223 as beam screen internal coating is mainly dictated by possible cryogenic needs to operate the beam screen at (or above) 80 K [2]. Under such circumstances, at the required magnetic fields of 14 T, no other superconducting candidates exist. Thus, only a comparison with  $R_s$  of copper can be tentatively provided.

The surface resistance  $R_s$  of Cu at 80 K can be estimated from the dc resistivity:  $R_s = \sqrt{2\pi f \mu_0 \rho_{dc}}/2$ . Using values for Cu with RRR = 70 [18], as foreseen for FCC [2], at 24.2 GHz one gets  $R_{s,Cu}(80 \text{ K}) \simeq 15 \text{ m}\Omega$  (we neglect a weak magnetic field dependence). Figure 4 yields for Tl-1223 at 80 K and 12 T  $R_s \simeq 190 \text{ m}\Omega$  in Sample II. It is difficult to directly compare those numbers, because the penetration depth at 12 T can exceed the film thickness, thus increasing the value of  $R_s$  with respect to a thicker film [10]. Moreover, in the mixed state the penetration depth is a complex quantity [19], which depends on the flux density in a nontrivial way. Adding the fact that the films are only at the beginning of the optimization process for high-frequency vortex pinning, it is not unreasonable that optimized, thicker films of Tl-1223 could outperform Cu for the FCC beam screen application. Clearly, additional work beyond this first report is necessary.

## VI. Conclusion

In this paper we have presented first, preliminary microwave measurements performed on two Tl-1223 samples, produced at different stages of the optimization of the growth process. Samples with  $T_c = 118$  K, indicating Tl-1223 phase, were successfully grown. The surface resistance  $R_s$  has been measured by varying the temperature in zero and fixed magnetic field, or by varying the applied field at fixed temperature. With the improvement of the deposition process the signatures of other phases were no longer detected, and a reduction by a factor  $\sim 10$  in  $R_s$  and  $\rho_n$  was obtained. The improvement of the deposition process brought as a consequence a much stronger resilience to the application of a dc magnetic

field, a required feature for perspective applications of Tl-1223 as a superconducting coating for the FCC beam screen. Future work will be devoted to a more extensive characterization of the field-dependent surface impedance, in view of the extraction of the characteristic microscopic vortex state parameters, for an accurate comparisons of the performances with other superconductors.

### References

- [1] M. Benedikt, V. Mertens, F. Cerutti et al., "FCC-hh: The hadron collider future circular collider conceptual design report volume 3," *Eur. Phys. J. Spec. Top.*, vol. 228, no. CERN-ACC-2018-0058, pp. 755–1107, 2018. [Online]. Available: <https://doi.org/10.1140/epjst/e2019-900087-0>
- [2] M. Benedikt, F. Zimmermann, B. Auchmann et al., "Future circular collider feasibility study report: Volume 2, accelerators, technical infrastructure and safety," *The European Physical Journal Special Topics*, vol. 234, p. 5713–6197, 2025. [Online]. Available: <https://doi.org/10.1140/epjs/s11734-025-01967-4>
- [3] S. Calatroni, "HTS coatings for impedance reduction in particle accelerators: Case study for the FCC at CERN," *IEEE Transactions on Applied Superconductivity*, vol. 26, no. 3, pp. 1–4, 2016. [Online]. Available: <https://doi.org/10.1109/TASC.2016.2520079>
- [4] S. Calatroni, E. Bellingeri, C. Ferdeghini, M. Putti, R. Vaglio, T. Baumgartner, and M. Eisterer, "Thallium-based high-temperature superconductors for beam impedance mitigation in the Future Circular Collider," *Superconductor Science and Technology*, vol. 30, no. 7, p. 075002, 2017. [Online]. Available: <https://doi.org/10.1088/1361-6668/aa6bd0>
- [5] A. Leveratto, A. Saba, S. Holleis, M. Himmerlich, B. Henrist, S. Fernandez-Pena, A. Moros, J. Bernardi, M. Eisterer, C. Bernini et al., "Future Circular Collider beam screen: progress on Tl-1223 HTS coating," *Superconductor Science and Technology*, vol. 33, no. 5, p. 054004, 2020. [Online]. Available: <https://doi.org/10.1088/1361-6668/ab7fbd>
- [6] A. Leveratto, A. Saba, C. Bernini, F. Loria, M. Cialone, A. Malagoli, S. Calatroni, and E. Bellingeri, "HTS for Future Circular Collider beamscreen: New moderate high-pressure reaction for the synthesis of Tl-1223," *IEEE Transactions on Applied Superconductivity*, vol. 35, no. 5, pp. 1–5, 2025. [Online]. Available: <https://doi.org/10.1109/TASC.2025.3549739>
- [7] S. Phok, P. Galez, J. Jorda, Z. Supardi, D. De Barros, P. Odier, A. Sin, and F. Weiss, "Tl- and (Hg,Re)-1223 oxide films by spray pyrolysis for practical applications," *Physica C: Superconductivity*, vol. 372-376, pp. 876–879, 2002. [Online]. Available: [https://doi.org/10.1016/S0921-4534\(02\)00886-9](https://doi.org/10.1016/S0921-4534(02)00886-9)
- [8] X. Liang, L. Ji, T. Li, J. Chen, H. Zhao, Q. Yang, M. He, M. Feng, X. Ming, H.-H. Wen, and C. Zeng, "Synthesis of Tl-2223 films, and their, microstructures, superconducting, magnetic, and microwave properties," *Journal of Alloys and Compounds*, vol. 983, p. 173825, 2024. [Online]. Available: <https://doi.org/10.1016/j.jallcom.2024.173825>
- [9] L. Chen, C. Ong, C. Neo, V. Varadan, and V. Varadan, *Microwave Electronics: Measurement and Materials Characterization*. Wiley, 2004. [Online]. Available: <https://books.google.it/books?id=1vmUdUX1BNIC>
- [10] N. Pompeo, A. Alimenti, K. Torokhtii, P. V. García, and E. Silva, "Substrate and finite-thickness-induced uncertainties in surface impedance measurements of thin conducting films," *IEEE Transactions on Instrumentation and Measurement*, vol. 74, pp. 1–15, 2025. [Online]. Available: <https://doi.org/10.1109/TIM.2024.3509590>
- [11] E. H. Brandt, "Penetration of magnetic ac fields into type-II superconductors," *Phys. Rev. Lett.*, vol. 67, pp. 2219–2222, Oct 1991. [Online]. Available: <https://link.aps.org/doi/10.1103/PhysRevLett.67.2219>
- [12] N. Pompeo and E. Silva, "Reliable determination of vortex parameters from measurements of the microwave complex resistivity," *Phys. Rev. B*, vol. 78, no. 9, p. 094503, 2008. [Online]. Available: <https://doi.org/10.1103/PhysRevB.78.094503>
- [13] A. Alimenti, K. Torokhtii, E. Silva, and N. Pompeo, "Challenging microwave resonant measurement techniques for conducting material characterization," *Meas. Sci. Technol.*, vol. 30, no. 6, p. 065601, 2019. [Online]. Available: <https://doi.org/10.1088/1361-6501/ab0e65>
- [14] N. Pompeo, K. Torokhtii, A. Alimenti, and E. Silva, "A method based on a dual frequency resonator to estimate physical parameters of superconductors from surface impedance measurements in a magnetic field," *Measurement*, vol. 184, p. 109937, 2021. [Online]. Available: <https://doi.org/10.1016/j.measurement.2021.109937>
- [15] R. Awad and N. H. Mohammed, "Synthesis and electrical resistivity studies of  $Tl_{1-x}Pr_xBa_2Ca_2Cu_3O_{9-\delta}$  superconductors," *Superconductor Science and Technology*, vol. 17, no. 1, p. 35, nov 2003. [Online]. Available: <https://doi.org/10.1088/0953-2048/17/1/006>
- [16] R. Awad, A. I. Abou-Aly, S. A. Mahmoud, and M. M. Barakat, "Thermal expansion measurements using x-ray powder diffraction of Tl-1223 substituted by molybdenum," *Superconductor Science and Technology*, vol. 20, no. 4, p. 401, mar 2007. [Online]. Available: <https://doi.org/10.1088/0953-2048/20/4/017>
- [17] A. Abou Aly, I. Ibrahim, R. Awad, A. El-Harizy, and A. Khalaf, "Stabilization of Tl-1223 phase by arsenic substitution," *Journal of superconductivity and novel magnetism*, vol. 23, no. 7, pp. 1325–1332, 2010. [Online]. Available: <https://doi.org/10.1007/s10948-010-0776-y>
- [18] S. Calatroni, "Materials & properties: Thermal & electrical characteristics," arXiv:2006.02842, 2020. [Online]. Available: <https://doi.org/10.48550/arXiv.2006.02842>
- [19] M. W. Coffey and J. R. Clem, "Unified Theory of Effects of Vortex Pinning and Flux Creep upon the rf Surface impedance of Type-II Superconductors," *Phys. Rev. Lett.*, vol. 67, no. 3, pp. 386–389, 1991. [Online]. Available: <https://doi.org/10.1103/PhysRevLett.67.386>